Calcif Tissue Int (2004) 75:15–22
DOI: 10.1007/s00223-004-0151-8

Calcified Tissue International

Technical Considerations for Microstructural Analysis of Human Trabecular Bone from Specimens Excised from Various Skeletal Sites

E. Nägele,[1,2] V. Kuhn,[1,2] H. Vogt,[1,2] T. M. Link,[3] R. Müller,[4] E.-M. Lochmüller,[2] F. Eckstein[1,5]

[1]Musculoskeletal Research Group, Institute of Anatomy, Ludwig-Maximilians-Universität München, Pettenkoferstr. 11, D-80336 München, Germany
[2]Universitatsfrauenklinik der Ludwig-Maximilians-Universität München, Innenstadt, Maistr. 11, D-80337 München, Germany
[3]Institute for Diagnostic Radiology, Klinikum rechts der Isar, Ismaningerstr. 22, D-81675 München, Germany
[4]Institute for Biomedical Engineering, Swiss Federal institute of Technology (ETH) and University of Zürich, Moussonstr. 18, CH-8044 Zürich, Switzerland
[5]Institute of Anatomy, Paracelsas Private Medical University, Müllner Hauptstr., Salzburg, Austria

Received: 25 June 2003 / Accepted: 29 December 2003 / Online publication: 25 March 2004

Abstract. The purpose of this study was to test the effect of repositioning, systematic displacements of the region of interest (ROI), and acquisition parameters (scan mode and integration time) on quantitative analysis of human trabecular bone microstructure at various skeletal sites, using microcomputed tomographic (μCT) technology. We investigated 28 cylindrical specimens of human trabecular bone (length 14 mm, diameter 8 mm) from four skeletal sites (femoral neck, greater trochanter, second lumbar vertebra, and distal radius). These specimens were selected from over 200 μCT measurements, in order to cover a large range of bone volume fraction (BV/TV) observed at each site. Cylindrical ROIs (length 6 mm, diameter 6 mm) were examined twice at an isotropic resolution of 26 μm, 8 weeks apart. In addition, comparative analyses were performed for displacements of the volumes of interest (VOIs) by 1, 2, 3, and 4 mm (83.4%, 66.6%, 50%, and 33.3% overlap), respectively. Eventually, comparative measurements were obtained at different resolution scan modes and integration times. The results show that μCT measurements are highly reproducible (range of the root mean square coefficient variation % (RMS CV%) = 0.64% to 1.29% for BV/TV at different sites). Displacements of the VOI of up to 4 mm generally led to non significant systematic differences in mean values of $<10\%$. When comparing various combinations of resolution scan modes and integration times, the use of an integration time of 100 ms was found to be preferable for determining microstructural parameters from human samples with this μCT scanner.

Key words: Trabecular bone — Microstructure — Microcomputed tomography — Human — Microarchitecture

Correspondence to: F. Eckstein; E-mail: eckstein@anat.med.uni-muenchen.de

Since microcomputed tomography has been introduced for quantitative measurement of cancellous bone [1–6], trabecular microstructure (or microarchitecture) is now accessible to direct, nondestructive analysis. As a virtue of its high isotropic resolution, microcomputed tomography permits three-dimensional (3D) morphometry without the imitations involved in sectional techniques that originate from two-dimensional (2D) model assumptions [6–8]. Changes in trabecular bone architecture are important in the context of age-related and osteoporotic bone loss [9–13], with the current definition of osteoporosis by the World Health Organization (WHO) including ''microstructural deterioration'' of trabecular architecture (i.e., http://www.nof.org/osteoporosis/stats.htm). It has been shown that knowledge of trabecular microstructure can improve the prediction of mechanical competence of cancellous bone compared with bone mass or density alone [14–18]. Moreover, bone microstructure has been shown to be amenable to therapeutic intervention in animal and human studies [19–24]. Alterations of bone microstructure have also been observed during pregnancy [25], in bone metastasis [26, 27], and in the subchondral bone region in osteoarthritis [28–32].

It has been suggested that a substantial heterogeneity of microstructural properties exists among various skeletal sites [8, 33–35], and that this heterogeneity also applies to different regions within the same bone [36, 37]. However, much remains to be understood about the determinants of human trabecular bone microstructure and mechanical competence, such as gender, age, and other factors.

The objective of the current study was to provide a methodological basis for studying human bone microstructure at various skeletal sites with use of microcomputed tomography. The study was designed to specifically assess the impact of repositioning (reproducibility), choice of volume of interest (VOI) (dis-

placement), and scanning parameters on excised human trabecular bone specimens. The analyses were performed in specimens that covered a wide range of bone volume fraction and structural morphology at each skeletal site in elderly subjects.

Materials and Methods

Specimens

The proximal femur, second lumbar vertebra (L2), and distal radius were harvested from 56 embalmed human cadavers that were used in a course of macroscopic anatomy (age range, 55 to 98 years; 27 women, 29 men). All bones were radiographed in 2 planes to exclude previous fracture. Although no fractures were observed in the femur and radius, 8 specimens with radiological signs of a fracture of L2 were discarded from the study.

Before the trabecular specimens were harvested, the orientation of the trabeculae in the femoral neck was determined from an anterior-posterior contact radiograph (Fig. 1A). A 14-mm planoparallel section was then obtained from the femoral neck using an Exact high-precision bandsaw (Exact Trennschleifsystem, Otto Herrmann, Norderstedt, Germany). The section was obtained in the middle of the femoral neck, perpendicular to the primary trabecular orientation of each individual femur (Fig. 1A). This section was radiographed again to identify the main trabecular bundle within the section (Fig. 1B). Eventually a cylindrical specimen with a diameter of 8 mm was retrieved at this site by using a diamond drill (Salzmann, München, Germany). In the trochanter, a 14-mm section was obtained (Fig. 1C) in a direction perpendicular to the direction of a fall on the greater trochanter (10° adduction, 15° internal rotation [38–40]). This section was radiographed (Fig. 1D), and a cylindrical specimen (dimensions noted previously) was then retrieved from the dense central region of the section, perpendicular to the slice and parallel to the impact direction during a fall on the side [38–40]. In the second lumbar vertebra, a full-length cylindrical specimen was obtained in the superior-inferior direction at 50% of the mediolateral diameter of the vertebra (middle), and at the transition of the anterior third (33%) and posterior two thirds (66%) of the anterior-posterior diameter. This location was selected to avoid the posterior venous plexus of the vertebral body. A 14-mm-long specimen was the obtained from the center (superior-inferior direction) of the full-length cylinder. In the distal radius, a 14-mm section was retrieved at the distal metaphysis, perpendicular to the long axis of the shaft. The distal end of the section was located 2 mm proximal to the wrist joint cavity [41], and a cylindrical specimen was finally obtained in the center of the section. In this way, we obtained 216 specimens for the four anatomic sites, which were stored in a solution of buffered formalin until microcomputed tomographic (μCT) scanning.

μCT Scanning

The scans were acquired for the central 6 mm of the specimen, using a μCT 20 scanner (Scanco Medical, Bassersdorf, Switzerland). In that system, a microfocus X-ray tube with a focal spot of 10 μm is used as a source. The filtered 40 kVp X-ray spectrum is peaked at 25 KeV allowing excellent bone versus soft tissue contrast owing to the pronounced photoelectric effect (for details see [5]). The resolution was set at 26 μm (isotropic), similar to that in a previous study on human trabecular bone [8]. Microstructural parameters are known to depend strongly on the spatial resolution. However, a previous study has suggested that up to a nominal resolution of 175 μm, structural parameters decrease or increase monotonously [42], so that the accurate values can be restored by using calibration procedures. The initial scans were performed in the "medium" scan mode and at an integration time of 100 ms. Medium scan mode means that 600 projections are taken over 216° (180° plus half the fan angle on either side). Each projection consists of 512 sample points, and tomographic images are reconstructed in 512×512 pixel matrices using standard convolution backprojection [4]. Integration time refers to the time that the detector is exposed to and "counting" incoming X-ray photons for a single projection. The total scan time per specimen was 4.1 hours when using these acquisition parameters.

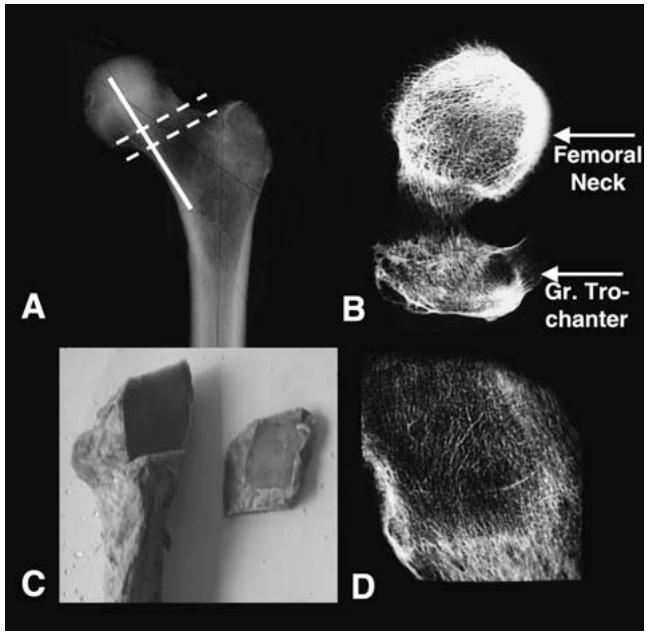

Fig. 1. Retrieval of planoparallel slice from femoral neck, perpendicular to the individual alignment of trabeculae (**A**) and radiograph of this slice (**B**), to obtain bone sample for microcomputed tomographic (μCT) analysis. Retrieval of planoparallel slice from greater femoral trochanter, perpendicular to the fall direction (**C**) and radiograph of this slice (**D**), to obtain bone sample for μCT analysis.

Within a defined VOI (diameter 6 mm and length 6 mm) we determined the following 3D structural parameters by using the following settings (Sigma 0.8; Support 1.0; Threshold 22 % of maximal gray value) and the software provided by the manufacturer. (1) bone volume fraction (BV/TV) in %; (2) trabecular number (Tb.N*) in 1/cm; (3) trabecular thickness (Tb.Th*) in μm; (4) trabecular separation (Tb.Sp*) in μm; (5) structure model index (SMI) [7], a measure of plate- or rod-like trabecular architecture; (6) connectivity density (Conn.D) in $1/mm^3$; and (7) degree of anisotropy (DA). It should be noted that all parameters were computed in a direct 3D fashion, without any model assumptions required for 2D analysis [8].

At each of these 4 anatomic sites we selected 7 specimens (28 in total) from the 48 to 56 measurements at each site. This was done to cover a wide range of BV/TV and structural parameters in elderly subjects. We selected the specimen with the second highest and second lowest values and divided the difference into 6 equidistant intervals. Specimens with the closest BV/TV value were then chosen to cover the entire range of values (Fig. 2). Note that the selection was made for each site, so that the 28 specimens did not originate from seven identical but from different donors.

The 28 specimens were examined again 8 weeks later, and the central 10 mm of each cylinder was scanned, with the settings specified previously. In a first step, a central VOI (diameter 6 mm, length 6 mm) was analyzed to evaluate the reproducibility of the scanning procedure. To evaluate the effect of slight displacements of the VOI within the cylinder, additional VOIs were analyzed 1 mm and 2 mm above, and

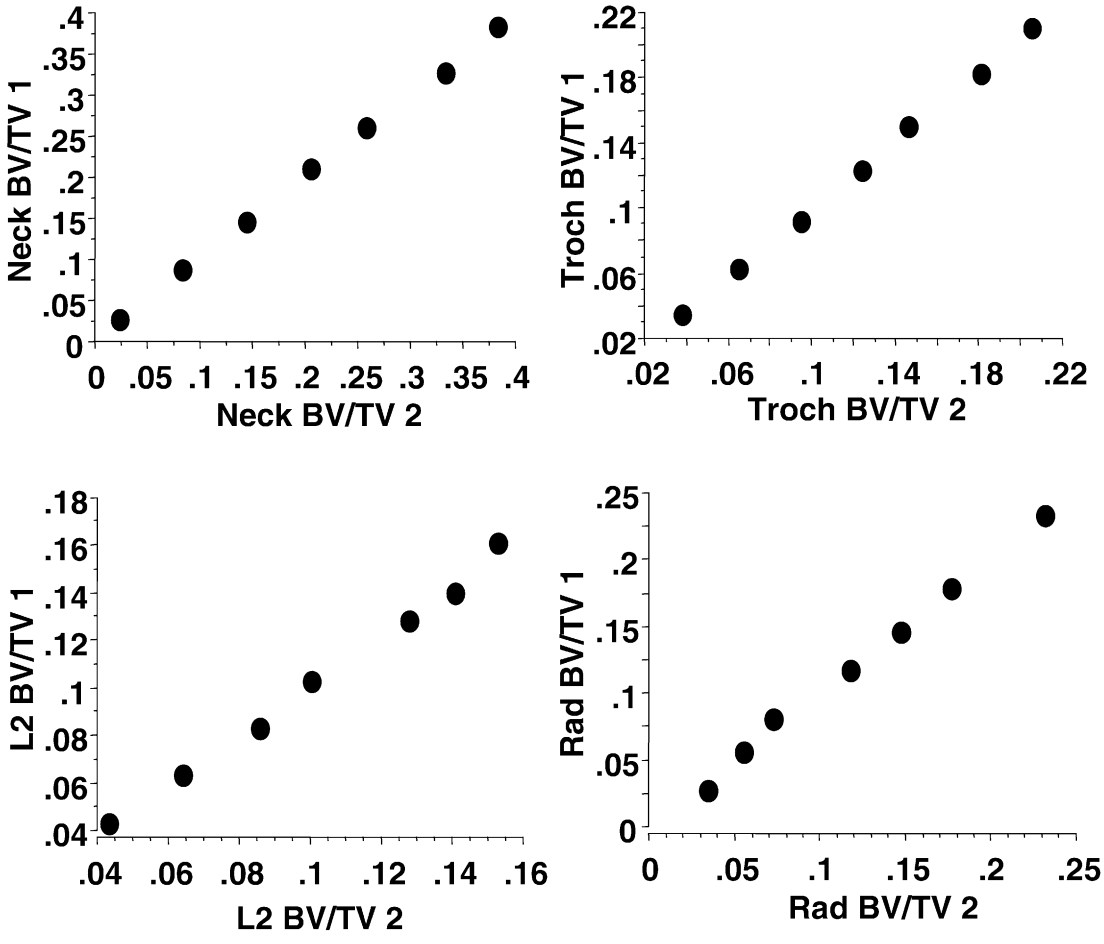

Fig. 2. Scatterplot showing the linear relationship of BV/TV for two measurements taken 8 weeks apart at the femoral neck, greater femoral trochanter, L2, and distal radius, and showing the range of BV/TV (second lowest to second highest) at each site.

1 mm and 2 mm below the central VOI. This procedure was performed to simulate the variability associated with retrieving the specimens from the bones.

To evaluate the effect of variations in scan time and scanning parameters, additional scans were obtained at medium scan mode and 50 ms integration time (scan time = 2.1 hours), at low scan mode and 100 ms integration time (scan time = 2.3 hours), and at low scan mode and 50 ms integration time (scan time = 1.2 hours). Considerable noise was noted in the scans made with low scan mode and 50 ms integration time, requiring adjustments of Sigma (1.2) and Support (2.0). Under these conditions, significant changes were observed in the BV/TV (in comparison with other scan modes and integration times), so that no comparison of structural parameters was eventually performed for these particular scanning conditions.

Statistical Analysis

To assess the reproducibility of the scanning procedure, we evaluated the systematic and random difference for the two measurements, as well as the root mean square coefficient of variation (RMS CV%) [43]. The random difference was assessed by taking the mean of the pairwise differences after eliminating the +/− signs, and the significance of the systematic difference was evaluated with a paired Student's *t*-test. To assess the relationship between the precision error and density (BV/TV), we determined the correlation coefficient between the SD and the baseline BV/TV and between the CV% and BV/TV across all specimens. To assess the effect of VOI displacement, measurements obtained 1 mm above the center, at the center, 1 mm below the center, and 2 mm below the center were compared to those at 2 mm above the center. The systematic and random differences were then evaluated for displacements of 1, 2, 3, and 4 mm, respectively, with the displacement corresponding to 83.4%, 66.6%, 50%, and 33.3% overlap of the analyzed VOI, respectively. To assess the relationship between the effect of VOI displacement and density (BV/TV), we determined the correlation coefficient between the absolute change and the baseline BV/TV and between the relative change (%) and the BV/TV across all specimens.

To assess the effect of scanning parameters, we also determined the systematic and random differences in relation to the medium scan mode with 100 ms integration time. For all types of analyses, we also performed linear regression analyses (Pearson correlation coefficient [r] and standard error of the estimate [SEE]), to determine whether the linear relationship between measurements was critically affected.

Results

Figure 3 displays 3D, microstructural reconstructions of trabecular specimens, visualizing the variation in BV/TV at each site. Table 1 reports the mean values, standard deviation, and range of structural characteristics of the first measurement in the 7 specimens at each site.

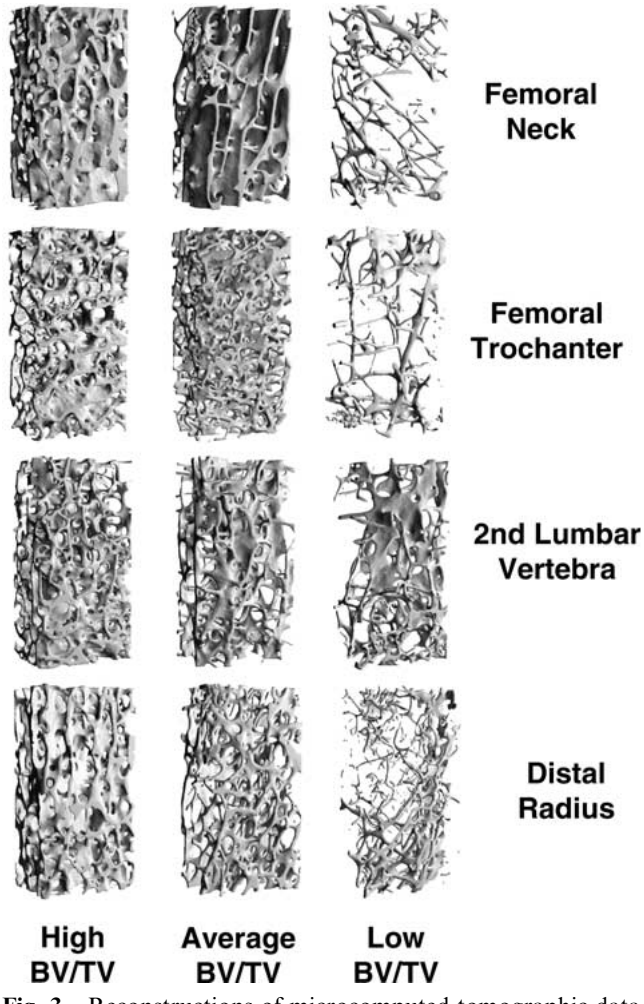

Fig. 3. Reconstructions of microcomputed tomographic data sets, including specimens with second highest, closest to average, and second lowest BV/TV at each site.

Table 2 reports the precision error of repeated measurement as the random difference, the RMS CV%, the linear regression coefficients, and the SEE (%) between the first and second measurement. No significant systematic change was observed between the first and second scan. The RMS CV% ranged from 0.24% (DA at L2) to 4.2% (Tb.Sp* at L2); the second measurement displayed a high linear relationship with the first one (Table 2). There was a negative correlation between the RMS CV% and the BV/TV ($r = -0.33$), but the correlation coefficient failed to reach statistical significance. The correlation between the RMS SD of repealed measurements and the BV/TV ($r = -0.04$) was close to zero.

The displacement of the volume of interest did not generally lead to a significant alteration in structural parameters (Table 3). Exceptions were Tb.N* at the greater trochanter (1–4 mm), Tb.Th* at L2 (4 mm), Tb.N* at the distal radius (3 and 4 mm), and Tb.Sp* at the distal radius (4 mm). No significant systematic differences were observed for Conn.D and DA (data not shown). The systematic differences encountered with a 4 mm displacement did, in general, not exceed 10%. Also, the structural data maintained a high linear relationship for displacements, with the strongest deviation from linearity being observed for the Tb.Th* ($r = 0.76$) and the SMI ($r = 0.82$) at the greater trochanter. A moderate deviation from linearity was also observed for DA at L2 ($r = 0.75$ for 4 mm) and strong deviations for DA at the greater trochanter ($r = 0.39$ for 3 mm, and $r = 0.17$ for 4 mm). There was no significant correlation between the random change in BV/TV (displacement) and the baseline BV/TV (neither for absolute nor for percentage change).

Variation of scanning parameters resulted in smaller systematic and random differences compared with displacement of the VOI (Table 4). When comparing both the low scan mode at 100 ms integration time acquisition as well as the medium scan mode at 50 ms integration time acquisition (scan time for both ~2 hours) with the medium scan mode at 100 ms acquisition, deviations for structural parameters (but not for BV/TV) were generally smaller for the low scan mode at 100 ms integration time acquisition.

Discussion

Microcomputed tomography is an evolving technique with the important advantage that measurements can be performed without destroying the specimens [5, 6]. Another strength of microcomputed tomography is that direct 3D measurements of bone microstructure can be derived, without the model assumptions that apply to 2D measurements with conventional bone histomorphometry. In order to evaluate the reliability of microstructural measurements in human trabecular bone with use of microcomputed tomography, we examined the precision of the measurements by repeating the scan several weeks later (reproducibility). In addition, we analyzed the effect of variability in sampling location and the effect of using various combinations of scanning parameters.

Only 28 samples were repeatedly investigated during this study. However, these were selected from over 200 measurements to cover a wide range of BV/TV and structural parameters observed at each skeletal site in elderly persons. This approach was chosen to render the analysis representative of the entire range of values observed at each site. The anatomical sites were selected to represent the most important locations of clinical fracture in osteoporosis, namely the proximal femur, the spine, and the distal forearm [44].

For the femoral neck, we followed the recommendations of Morgan and Keaveny [45] for obtaining the trabecular bone samples. Particular care was taken to retrieve specimens precisely from the trabecular bundle

Table 1. Baseline characteristics of the microstructural properties of the specimens examined at various skeletal sites

Parameter	Femoral Neck	Femoral trochanter	L2	Distal radius
BV/TV (%)	20.6 ± 12.8 (2.34–38.3)	12.2 ± 6.08 (3.50–21.1)	10.2 ± 4.07 (4.31–16.4)	12.0 ± 7.10 (2.78–23.4)
Tb.N* (1/cm)	10.9 ± 3.29 (5.47–16.3)	11.8 ± 2.98 (7.62–14.7)	9.87 ± 1.65 (8.10–12.1)	11.8 ± 1.24 (9.87–13.6)
Tb.Th* (μm)	207 ± 57 (123–281)	143 ± 23 (119–174)	140 ± 14 (124–159)	148 ± 26 (106–180)
Tb.Sp* (μm)	951 ± 417 (703–1840)	850 ± 263 (624–1282)	986 ± 177 (764–1210)	792 ± 113 (654–1003)
SMI	1.01 ± 0.80 (−0.17–2.02)	1.76 ± 0.51 (1.11–2.50)	1.71 ± 0.61 (0.62–2.44)	2.01 ± 0.82 (0.67–3.22)
Conn.D ($1/mm^3$)	3.05 ± 2.82 (0.60–6.92)	3.35 ± 1.62 (0.85–5.00)	2.18 ± 0.98 (1.12–3.38)	2.37 ± 1.11 (0.58–4.15)
DA	2.31 ± 0.61 (1.36–2.79)	1.65 ± 0.19 (1.41–1.95)	1.50 ± 0.29 (1.15–1.97)	1.88 ± 0.45 (1.50–2.55)

Data are mean ± SD (range)
BV/TV, bone volume fraction; Tb.N, trabecular number; Tb.Th., trabecular thickness; Tb.Sp., trabecular separation; SMI, structure model index; Conn.D, connectivity density; DA, degree of anisotropy
*Derived from three-dimensional μCT data without model assumptions required for 2D analysis, i.e., histomorphometry

Table 2. Reproducibility of microstructural analysis of human trabecular bone at various skeletal sites

	Fem neck		Fem trochanter		L2		Distal radius	
Parameter	Diff (RMSCV%)	Corr (SEE)	Diff (RMSCV%)	Corr (SEE)	Diff (RMSCV%)	Corr (SEE)	Diff (RMSCV%)	Corr (SEE)
BV/TV	0.32 (0.73)	1.00 (0.00)	0.28 (0.68)	1.00 (0.00)	0.22 (0.64)	1.00 (0.00)	0.29 (1.29)	1.00 (0.00)
Tb.N*	0.10 (0.25)	1.00 (0.01)	0.01 (0.32)	1.00 (0.01)	0.13 (0.35)	1.00 (0.01)	0.15 (0.35)	0.99 (0.02)
Tb.Th*	3.79 (2.73)	1.00 (0.00)	2.10 (1.63)	1.00 (0.00)	1.14 (0.86)	0.99 (0.00)	3.64 (3.75)	0.95 (0.01)
Tb.Sp*	12.5 (2.93)	1.00 (0.00)	13.6 (1.62)	1.00 (0.02)	17.1 (4.19)	0.99 (0.02)	12.3 (3.73)	1.00 (0.01)
SMI	0.06 (1.26)	1.00 (0.05)	0.04 (0.39)	1.00 (0.06)	0.06 (0.55)	0.99 (0.11)	0.04 (0.26)	1.00 (0.02)
Conn.D	0.36 (2.03)	0.99 (0.49)	0.10 (0.44)	1.00 (0.14)	0.10 (0.53)	0.99 (0.11)	0.12 (1.08)	0.99 (0.13)
DA	0.10 (0.76)	0.97 (0.17)	0.04 (0.27)	0.96 (0.06)	0.03 (0.24)	0.99 (0.05)	0.05 (0.43)	0.99 (0.07)

Fem, femoral; Diff, mean random difference; RMSCV%, root mean square average coefficient of variation; Corr, Pearson correlation coefficient; SEE, standard error of the estimate; BV/TV, bone volume fraction; Tb.N, trabecular number; Tb.Th., trabecular thickness; Tb.Sp., trabecular separation; SMI, structure model index; Conn.D, connectivity density; DA, degree of anisotropy
*Derived from three-dimensional μCT data without model assumptions required for 2D analysis, i.e., histomorphometry

that extends from the femoral head to the medial femoral cortex. This was done to obtain a reproducible anatomic site for measurement, and to avoid areas with extensive bone resorption, such as Wards triangle. Note that no intact trabecular specimens can be obtained at this location in subjects with low BV/TV. Particular care was also taken to retrieve the specimens according to the individual orientation of the trabeculae at the neck, as this orientation can vary substantially between subjects and deviates considerably from the macroscopic anatomic axes of the femoral neck [46].

Differences in structural parameters were small when repeating the measurements, and were in the same order of magnitude as those resulting from minimal displacement of the sample. This finding indicates that the reproducibility is most likely limited by ability to select a certain VOI, and not by the reproducibility of the physical measurement itself.

Some differences were observed when systematically shifting the VOI through the cylindrical specimen, simulating variability associated with sampling the specimens. However, a high linear relationship was maintained for most parameters. Our data suggest that care must be taken when selecting the anatomical measurement location at the greater femoral trochanter and in the vertebral body (especially for DA). Relatively strong deviations were observed at these sites with varying the depth of the VOI relative to the bone surface [47]. It is clear that the spatial sampling error would be >4 mm for biopsies taken *in vivo* (i.e., from the iliac crest). However, we feel that displacements in the range of 1 to 4 mm adequately reflect the sampling error associated with trabecular specimens obtained from ex-

Table 3. Effect of displacements of 1,2,3 and 4 mm on microstructural analysis of a 10 mm sample of human trabecular bone

	Fem neck		Fem Trochanter		L2		Distal radius	
Parameter/ displacement	Syst (Rand) Diff	Corr (SEE)	Syst (Rand) Diff	Corr (SEE)	Syst (Rand) Diff	Corr (SEE)	Syst (Rand) Diff	Corr (SEE)
BV/TV								
1 mm	+0.58 (0.70)	1.00 (0.01)	−0.10 (0.60)	0.99 (0.01)	+0.15 (0.23)	1.00 (0.00)	−0.13 (0.29)	1.00 (0.00)
2 mm	+1.23 (1.51)	0.99 (0.02)	−0.40 (1.01)	0.98 (0.01)	+0.06 (0.38)	0.99 (0.01)	−0.27 (0.53)	1.00 (0.01)
3 mm	+2.07 (2.39)	0.98 (0.03)	−0.37 (1.29)	0.97 (0.02)	−0.11 (0.59)	0.98 (0.01)	−0.57 (0.80)	0.99 (0.01)
4 mm	+2.86 (3.21)	0.97 (0.03)	−0.37 (1.78)	0.95 (0.02)	−0.38 (0.88)	0.95 (0.01)	−0.85 (1.12)	0.99 (0.01)
Tb.N* (1/cm)								
1 mm	+0.01 (0.10)	1.00 (0.01)	−0.16[a] (0.19)	1.00 (0.02)	−0.03 (0.25)	0.98 (0.04)	−0.14 (0.20)	1.00 (0.01)
2 mm	+0.23 (0.23)	1.00 (0.02)	−0.30[b] (0.30)	1.00 (0.02)	−0.10 (0.31)	0.97 (0.05)	−0.21 (0.27)	0.99 (0.02)
3 mm	+0.41 (0.41)	1.00 (0.03)	−0.47[a] (0.47)	1.00 (0.03)	+0.04 (0.41)	0.95 (0.06)	−0.37[a] (0.41)	0.98 (0.03)
4 mm	+0.67 (0.67)	0.99 (0.05)	−0.48 (0.67)	0.98 (0.06)	+0.21 (0.44)	0.96 (0.05)	−0.51[a] (0.51)	0.98 (0.03)
Tb.Th*(μm)								
1 mm	−2.31 (7.54)	0.99 (0.01)	+1.84 (3.16)	0.99 (0.00)	+0.21 (1.41)	0.99 (0.00)	+0.36 (2.19)	1.00 (0.00)
2 mm	−0.73 (15.30)	0.96 (0.02)	+3.67 (6.79)	0.93 (0.01)	−0.84 (2.21)	0.98 (0.00)	+0.16 (4.01)	0.98 (0.00)
3 mm	+4.16 (21.21)	0.94 (0.02)	+5.09 (9.37)	0.86 (0.01)	−1.76 (3.10)	0.98 (0.00)	+1.53 (6.04)	0.97 (0.01)
4 mm	+7.40 (25.20)	0.91 (0.02)	+5.37 (10.91)	0.76 (0.02)	−4.00[a] (4.97)	0.96 (0.00)	+2.33 (8.50)	0.93 (0.01)
Tb.Sp*(μm)								
1 mm	+6.81 (15.67)	1.00 (0.01)	+11.2 (18.1)	1.00 (0.02)	+3.24 (29.2)	0.97 (0.04)	+8.30 (12.0)	1.00 (0.01)
2 mm	−23.4 (23.4)	1.00 (0.03)	+21.2 (28.5)	0.99 (0.03)	+13.8 (31.9)	0.97 (0.05)	+12.7 (18.9)	0.99 (0.01)
3 mm	−49.1 (49.1)	1.00 (0.04)	+27.4 (36.9)	0.99 (0.04)	+3.31 (38.9)	0.96 (0.05)	+24.3 (28.8)	0.99 (0.02)
4 mm	−84.7 (84.7)	0.99 (0.05)	+23.9 (39.1)	0.99 (0.04)	−15.3 (44.7)	0.96 (0.06)	+37.3[b] (37.3)	0.98 (0.02)
SMI								
1 mm	−0.05 (0.09)	0.99 (0.12)	+0.07 (0.11)	0.98 (0.12)	−0.03 (0.08)	0.99 (0.10)	0.03 (0.06)	1.00 (0.07)
2 mm	−0.09 (0.17)	0.96 (0.24)	+0.15 (0.20)	0.94 (0.19)	−0.02 (0.15)	0.94 (0.22)	0.05 (0.11)	0.99 (0.12)
3 mm	−0.16 (0.23)	0.93 (0.35)	+0.19 (0.26)	0.87 (0.28)	+0.01 (0.19)	0.90 (0.30)	0.10 (0.15)	0.98 (0.16)
4 mm	−0.26 (0.33)	0.88 (0.48)	+0.21 (0.32)	0.82 (0.35)	+0.07 (0.22)	0.87 (0.34)	0.16 (0.18)	0.98 (0.17)

[a] ($p < 0.05$); [b] ($p < 0.01$) Syst, systematic differences; Rand, random difference; other abbreviations as in Tables 1 and 2

Table 4. Effect of acquisition parameters (mode/integration time) and scan time on microstructural analysis of human trabecular bone

	Fem neck		Fem Trochanter		L2		Distal radius	
Parameter/ displacement	Syst (Rand) Diff	Corr (SEE)	Syst (Rand) Diff	Corr (SEE)	Syst (Rand) Diff	Corr (SEE)	Syst (Rand) Diff	Corr (SEE)
BV/TV (%)								
LR 100	+0.10 (0.16)	1.00 (0.00)	+0.10* (0.10)	1.00 (0.00)	+0.02 (0.10)	1.00 (0.00)	+0.07* (0.07)	1.00 (0.00)
MR 50	+0.04 (0.13)	1.00 (0.00)	+0.05 (0.05)	1.00 (0.00)	−0.03 (0.06)	1.00 (0.00)	−0.07 (0.09)	1.00 (0.00)
Tb.N*(1/cm)								
LR 100	+0.31 (0.32)	1.00 (0.04)	+0.04 (0.09)	1.00 (0.01)	+0.05 (0.08)	1.00 (0.01)	+0.03 (0.20)	0.99 (0.03)
MR 50	+1.21 (1.21)	0.97 (0.14)	+0.20[a] (0.20)	1.00 (0.02)	+0.11[a] (0.11)	1.00 (0.00)	+0.10 (0.29)	0.97 (0.04)
Tb.Th*(μm)								
LR 100	+0.99 (1.81)	1.00 (0.00)	+0.80[a] (0.91)	1.00 (0.00)	+0.40 (1.00)	1.00 (0.00)	+1.99 (1.99)	0.99 (0.00)
MR 50	−2.09 (2.46)	1.00 (0.00)	−0.29 (0.63)	1.00 (0.00)	−0.67[a] (0.70)	1.00 (0.00)	+1.14 (1.60)	0.99 (0.00)
Tb.Sp*(μm)								
LR 100	−8.23 (8.26)	1.00 (0.01)	−2.24 (5.13)	1.00 (0.01)	−9.19 (9.84)	1.00 (0.01)	+2.57 (8.31)	0.99 (0.01)
MR 50	−21.3 (21.3)	1.00 (0.03)	−5.01[a] (5.27)	1.00 (0.00)	−3.11[a] (3.11)	1.00 (0.00)	+3.80 (14.3)	0.99 (0.02)
SMI								
LR 100	+0.01 (0.03)	1.00 (0.03)	+0.00 (0.01)	1.00 (0.01)	+0.01 (0.01)	1.00 (0.01)	+0.01 (0.02)	1.00 (0.03)
MR 50	+0.09 (0.09)	0.98 (0.17)	+0.00 (0.01)	1.00 (0.01)	+0.00 (0.00)	1.00 (0.01)	+0.01 (0.02)	1.00 (0.04)
Conn.D (1/mm^3)								
LR 100	+0.33 (0.34)	1.00 (0.16)	+0.00 (0.04)	1.00 (0.06)	+0.00 (0.02)	1.00 (0.04)	+0.01 (0.05)	1.00 (0.05)
MR 50	+1.17 (1.17)	1.00 (0.43)	+0.03 (0.06)	1.00 (0.09)	+0.02 (0.03)	1.00 (0.03)	−0.04 (0.09)	0.98 (0.18)

MR, medium resolution; LR, low resolution; 100, integration time of 100 ms; 50, integration time of 50 ms; other abbreviations as in Tables 1, 2, 3
[a] $P < 0.05$; [b] $P < 0.01$

cised bones under radiographic control, as in this *ex vivo* study.

With respect to the scanning parameters, it is obviously best to use the highest scan mode and longest integration time. However, this is at the expense of the scan time, which may limit the throughput in large-scale studies. Our results show that low scan mode and 50 ms integration time lead to considerable noise, which would require adjustment in filter settings and the threshold to arrive at the same BV/TV. We thus recommend use of an integration time of at least 100 ms, potentially in combination with a low scan mode, but preferably with a medium scan mode. In this context one must be aware that the most recent generation of μCT scanners can acquire data sets at much faster scan times than the system used for this study.

In conclusion, the current methodological study suggests that analysis of human trabecular microarchitecture with microcomputed tomography is highly reproducible. The variability in structural parameters associated with small variability of the sampling site on excised bones is low, but depends on the specific anatomic location. When comparing various combinations of resolution scan modes and integration times, the use of an integration time of 100 ms was found to be preferable for determining microstructural parameters from human samples with this μCT scanner.

Acknowledgment. We thank Drs. Bruno Koller and Andres Laib (Scanco Medical) for their valuable advice.

References

1. Feldkamp LA, Goldstein SA, Parfitt AM, Jesion G, Kleerekoper M (1989) The direct examination of three-dimensional bone architecture *in vitro* by computed tomography. J Bone Miner Res 4:3–11
2. Kuhn JL, Goldstein SA, Feldkamp LA, Goulet RW, Jesion G (1990) Evaluation of a microcomputed tomography system to study trabecular bone structure. J Orthop Res 8:833–842
3. Durand EP, Rüegsegger P (1992) High-contrast resolution of CT images for bone structure analysis. Med Phys 19:569–573
4. Rüegsegger P, Koller B, Müller R (1996) A microtomographic system for the nondestructive evaluation of bone architecture. Calcif Tissue Int 58:24–29
5. Müller R, Rüegsegger P (1997) Micro-tomographic imaging for the nondestructive evaluation of trabecular bone architecture. Stud Health Technol Inform 40:61–79
6. Odgaard A (1997) Three-dimensional methods for quantification of cancellous bone architecture. Bone 20:315–328
7. Hildebrand T, Rüegsegger E (1997) Quantification of bone microarchitecture with the structure model index. Comp Meth Biomech Biomed Eng 1:15–23
8. Hildebrand T, Laib A, Müller R, Dequeker J, Rüegsegger P (1999) Direct three-dimensional morphometric analysis of human cancellous bone: microstructural data from spine, femur, iliac crest, and calcaneus. J Bone Miner Res 14:1167–1174
9. Genant HK, Gordon C, Jiang Y, Link TM, Hans D, Majumdar S, Lang TF (2000) Advanced imaging of the macrostructure and microstructure of bone. Horm Res 54(Suppl 1): 24–30
10. Legrand E, Chappard D, Pascaretti C, Duquenne M, Krebs S, Rohmer V, Basle MF, Audran M (2000) Trabecular bone microarchitecture, bone mineral density, and vertebral fractures in male osteoporosis. J Bone Miner Res 15:13–19
11. Ding M, Odgaard A, Linde F, Hvid I (2002) Age-related variations in the microstructure of human tibial cancellous bone. J Orthop Res 20:615–621
12. Dalle CL, Arlot ME, Chavassieux PM, Roux JP, Portero NR, Meunier PJ (2001) Comparison of trabecular bone microarchitecture and remodeling in glucocorticoid-induced and postmenopausal osteoporosis. J Bone Miner Res 16:97–103
13. Ciarelli TE, Fyhrie DP, Schaffler MB, Goldstein SA (2000) Variations in three-dimensional cancellous bone architecture of the proximal femur in female hip fractures and in controls. J Bone Miner Res 15:32–40
14. Ulrich D, Hildebrand T, Van Rietbergen B, Müller R, Rüegsegger P (1997) The quality of trabecular bone evaluated with micro-computed tomography, FEA and mechanical testing. Stud Health Technol Inform 40:97–112
15. Ulrich D, Van Rietbergen B, Laib A, Rüegsegger P (1999) The ability of three-dimensional structural indices to reflect mechanical aspects of trabecular bone. Bone 25:55–60
16. Pistoia W, Van Rietbergen B, Lochmüller EM, Lill CA, Eckstein F, Rüegsegger P (2002) Estimation of distal radius failure load with micro-finite element analysis models based on three-dimensional peripheral quantitative computed tomography images. Bone 30:842–848
17. Van Rietbergen B, Odgaard A, Kabel J, Huiskes R (1998) Relationships between bone morphology and bone elastic properties can be accurately quantified using high-resolution computer reconstructions. J Orthop Res 16:23–28
18. Müller R, Rüegsegger P (1996) Analysis of mechanical properties of cancellous bone under conditions of simulated bone atrophy. J Biomech 29:1053–1060
19. Lane NE, Kumer JL, Majumdar S, Khan M, Lotz J, Stevens RE, Klein R, Phelps KV (2002) The effects of synthetic conjugated estrogens, a (cenestin) on trabecular bone structure and strength in the ovariectomized rat model. Osteoporos Int 13:816–823
20. Lespessailles E, Poupon S, Niamane R, Loiseau-Peres S, Derommelaere G, Harba R, Courteix D, Benhamou CL (2002) Fractal analysis of trabecular bone texture on calcaneus radiographs: effects of age, time since menopause and hormone replacement therapy. Osteoporos Int 13:366–372
21. Ito M (2003) [Effects of bisphosphonate on trabecular microstructure.] Nippon Rinsho 61:213–218
22. Shiraishi A, Higashi S, Masaki T, Saito M, Ito M, Ikeda S, Nakamura T (2002) A comparison of alfacalcidol and menatetrenone for the treatment of bone loss in an ovariectomized rat model of osteoporosis. Calcif Tissue Int 71:69–79
23. Dempster DW, Cosman F, Kurland ES, Zhou H, Nieves J, Woelfert L, Shane E, Plavetic K, Muller R, Bilezikian J, Lindsay R (2001) Effects of daily treatment with parathyroid hormone on bone microarchitecture and turnover in patients with osteoporosis: a paired biopsy study. J Bone Miner Res 16:1846–1853
24. Jiang Y, Zhao J, Genant HK, Dequeker J, Geusens P (1998) Bone mineral density and biomechanical properties of spine and femur of ovariectomized rats treated with naproxen. Bone 22:509–504
25. Shahtaheri SM, Aaron JE, Johnson DR, Purdie DW (1999) Changes in trabecular bone architecture in women during pregnancy. Br J Obstet Gynaecol 106:432–438
26. Kurth AA, Muller R (2001) The effect of an osteolytic tumor on the three-dimensional trabecular bone morphology in an animal model. Skeletal Radiol 30:94–98

27. Tamada T (2000) [Three-dimensional microstructural analysis of human lumbar vertebrae using microcomputed tomography in bone metastasis from prostate cancer.] Nippon Igaku Hoshasen Gakkai Zasshi 60:740–751
28. Kamibayashi L, Wyss UP, Cooke TD, Zee B (1995) Trabecular microstructure in the medial condyle of the proximal tibia of patients with knee osteoarthritis. Bone 17:27–35
29. Beuf O, Ghosh S, Newitt DC, Link TM, Steinbach L, Ries M, Lane N, Majumdar S (2002) Magnetic resonance imaging of normal and osteoarthritic trabecular bone structure in the human knee. Arthritis Rheum 46:385–393
30. Patel V, Issever AS, Burghardt A, Laib A, Ries M, Majumdar S (2003) MicroCT evaluation of normal and osteoarthritic bone structure in human knee specimens. J Orthop Res. 21:6–13
31. Day JS, Ding M, van der Linden JC, Hvid I, Sumner DR, Weinans H (2001) A decreased subchondral trabecular bone tissue elastic modulus is associated with pre-arthritic cartilage damage. J Orthop Res 19:914–918
32. Boyd SK, Müller R, Zernicke RF (2002) Mechanical and architectural bone adaptation in early stage experimental osteoarthritis. J Bone Miner Res 17:687–694
33. Dempster DW, Ferguson-Pell MW, Mellish RW, Cochran GV, Xie F, Fey C, Herbert W, Parisien M, Lindsay R (1993) Relationships between bone structure in the iliac crest and bone structure and strength in the lumbar spine. Osteoporos Int 3:90–96
34. Amling M, Herden S, Posl M, Hahn M, Ritzel H, Delling G (1996) Heterogeneity of the skeleton: comparison of the trabecular microarchitecture of the spine, the iliac crest, the femur, and the calcaneus. J Bone Miner Res 11:36–45
35. Goldstein SA (1987) The mechanical properties of trabecular bone: dependence on anatomic location and function. J Biomech 20:1055–1061
36. Thomsen JS, Ebbesen EN, Mosekilde L (2002) Zone-dependent changes in human vertebral trabecular bone: clinical implications. Bone 30:664–669
37. Issever AS, Vieth V, Letter A, Meier N, Laib A, Newitt D, Majumdar S, Link TM (2002) Local differences in the trabecular bone structure of the proximal femur depicted with high-spatial-resolution MR imaging and multisection CT. Acad Radiol 9:1395–1406
38. Courtney AC, Wachtel EF, Myers ER, Hayes WC (1994) Effects of loading rate on strength of the proximal femur. Calcif Tissue Int 55:53–58
39. Courtney AC, Wachtel EF, Myers ER, Hayes WC (1995) Age-related reductions in the strength of the femur tested in a fall-loading configuration. J Bone Joint Surg Am 77:387–395
40. Bouxsein ML, Courtney AC, Hayes WC (1995) Ultrasound and densitometry of the calcaneus correlate with the failure loads of cadaveric femurs. Calcif Tissue Int 56:99–103
41. Lochmüller EM, Lill CA, Kuhn V, Schneider E, Eckstein F (2002) Radius bone strength in bending, compression, and falling and its correlation with clinical densitometry at multiple sites. J Bone Miner Res 17: 1629–1638
42. Müller R, Koller B, Hildebrand T, Laib A, Gianolini S, Rüegsegger P (1996) Resolution dependency of microstructural properties of cancellous bone based on three-dimensional μ-tomography. Technol Health Care 4:113–119
43. Glüer CC, Blake G, Lu Y, Blunt BA, Jergas M, Genant HK (1995) Accurate assessment of precision errors: how to measure the reproducibility of bone densitometry techniques. Osteoporos Int 5:262–270
44. Riggs BL, Melton LJ III (1995) The worldwide problem of osteoporosis: insights afforded by epidemiology. Bone 17:505S–511S
45. Morgan EF, Keaveny TM (2001) Dependence of yield strain of human trabecular bone on anatomic site. J Biomech 34:569–577
46. Turner CH, Cowin SC (1988) Errors induced by off-axis measurement of the elastic properties of bone. J Biomech Eng 110:213–215
47. Thomsen JS, Ebbesen EN, Mosekilde L (2002) Zone-dependent changes in human vertebral trabecular bone: clinical implications. Bone 30:664–669